

RSC Advances



This is an *Accepted Manuscript*, which has been through the Royal Society of Chemistry peer review process and has been accepted for publication.

Accepted Manuscripts are published online shortly after acceptance, before technical editing, formatting and proof reading. Using this free service, authors can make their results available to the community, in citable form, before we publish the edited article. This *Accepted Manuscript* will be replaced by the edited, formatted and paginated article as soon as this is available.

You can find more information about *Accepted Manuscripts* in the [Information for Authors](#).

Please note that technical editing may introduce minor changes to the text and/or graphics, which may alter content. The journal's standard [Terms & Conditions](#) and the [Ethical guidelines](#) still apply. In no event shall the Royal Society of Chemistry be held responsible for any errors or omissions in this *Accepted Manuscript* or any consequences arising from the use of any information it contains.

Thermal Decomposition Based Synthesis of Ag-In-S/ZnS Quantum Dots and Their Chlorotoxin-Modified Micelles for Brain Tumor Cell Targeting

Siqi Chen,^{a,b} Mojtaba Ahmadiantehrani,^c
Nelson G. Publicover,^{a,b} Kenneth W. Hunter Jr.,^{b,d} and Xiaoshan Zhu*^{a,b}

^a *Department of Electrical and Biomedical Engineering, University of Nevada, Reno, NV, USA*

^b *Biomedical Engineering Program, University of Nevada, Reno, NV, USA*

^c *Department of Chemical and Materials Engineering, University of Nevada, Reno, NV, USA*

^d *Department of Microbiology and Immunology, University of Nevada, Reno, NV, USA*

*To whom correspondence should be addressed. Email: xzhu@unr.edu. Phone: 1-775-682-6298.
Fax: 1-775-784-6627

ABSTRACT

Cadmium-free silver-indium-sulfide (Ag-In-S or AIS) chalcopyrite quantum dots (QDs) as well as their core-shell structures (AIS/ZnS QDs) are being paid significant attention in biomedical applications because of their low toxicity and excellent optical properties. Here we report a simple and safe synthetic system to prepare high quality AIS and AIS/ZnS QDs using thermal decomposition. The synthetic system simply involves heating a mixture of silver acetate, indium acetate, and oleic acid in dodecanethiol at 170 °C to produce AIS QDs with a 13% quantum yield (QY). After ZnS shell growth, the produced AIS/ZnS QDs achieve a 41% QY. To facilitate phase transfer and bioconjugation of AIS/ZnS QDs for cellular imaging, these QDs were loaded into the core of PLGA-PEG (5k:5k) based micelles to form AIS/ZnS QD-micelles. Cellular imaging studies showed that chlorotoxin-conjugated QD-micelles can be specifically internalized into U-87 brain tumor cells. This work discloses that the scalable synthesis of AIS/ZnS QDs and the facile surface/interface chemistry for phase transfer and bioconjugation of these QDs may open an avenue for the produced QD-micelles to be applied to the detection of endogenous targets expressed on brain tumor cells, or more broadly to cell- or tissue-based diagnosis and therapy.

INTRODUCTION

I-III-VI chalcopyrite quantum dots (QDs) such as copper-indium-sulfide (Cu-In-S or CIS) and silver-indium-sulfide (Ag-In-S or AIS) as well as their core-shell structures (CIS/ZnS and AIS/ZnS QDs), are emerging materials replacing the commonly available cadmium-based II-VI QDs for biomedical applications because they are of low toxicity and excellent optical

properties.¹⁻⁴ In spite of these merits, significant efforts are still needed to develop high quality I-III-VI QDs into broader biomedical applications especially for in vitro or in vivo sensing/imaging. Specifically, scalable syntheses of high quality I-III-VI QDs are desired because a large amount of bright I-III-VI QDs can be produced in a single synthetic reaction to sustain biomedical research for reliable experimental observation or data collection and also save synthesis costs. In addition, since I-III-VI QDs usually are synthesized in organic solvents and thus capped with hydrophobic ligands, facile surface/interface chemistries are required to render I-III-VI QDs water-dispersible and also to provide functional groups for subsequent bioconjugation with biological moieties.

In this work, we introduced a thermal decomposition based synthesis method for AIS QDs, which can be easily scaled up for QD production compared to hot-injection ones. Many recent reports have demonstrated the synthesis of AIS QDs.⁵⁻¹² Nevertheless, most of them adopted hot-injection methods. Although $\text{AgIn}(\text{S}_2\text{CN}(\text{C}_2\text{H}_5)_2)_4$ precursor was used for AIS synthesis in a thermal decomposition approach, the preparation of this precursor involved multiple wash/dry steps and the use of toxic sodium diethyldithiocarbamate.⁷ In our synthetic system, we simply heated a mixture of silver acetate, indium acetate, and oleic acid in dodecanethiol as the only solvent at 170 °C to produce AIS QDs. No complex precursors, additional sulfur sources, and other solvents are needed. All chemicals in this reaction are commercially available. In order to enhance the QD quantum yield (QY), we further grew a ZnS shell on AIS surface to form AIS/ZnS QDs with a 41% QY.

To demonstrate potential biomedical or biological applications of AIS/ZnS QDs, we loaded these QDs into the core of PLGA-PEG (5kDa:5kDa) based micelles to form the AIS/ZnS QD-micelles and further investigated their specific-targeting functionality as cellular imaging probes

or contrasts. With functional groups such as maleimide on PEG heads, we conjugated the QD-micelles with chlorotoxin (CTX), a ligand that specifically binds to U-87 brain tumor cells. Our cellular imaging studies showed that the QD-micelles conjugated with CTX are specifically internalized into the brain tumor cells. Since the hydrophobic core of micelles can be loaded with both drugs and image contrasts, the specific cellular internalization suggests that the QD-micelle structures could be important and versatile nanoplatforms for cell- or tissue-based diagnosis and therapy. Moreover, loading multiple QDs in the hydrophobic cores could avoid the blinking effect of single QD and therefore facilitate continuous image tracking. Notably, the common surface modification approaches using thiolated ligands to exchange hydrophobic ligands capped on QDs (CdSe or CdS) are less favorable for AIS/ZnS QDs.¹³⁻¹⁶ This is because I-III-VI QDs, including AIS/ZnS QDs, are usually capped with the strong coordinating ligand dodecanethiol which is hard to displace by other foreign thiols.¹⁷ Although some groups have reported the use of amphiphilic polymers to encapsulate QDs (CdSe or CdS), they need an overnight air-dry process followed by a heated film hydration, or a 24-hr dialysis to remove organic solvents or excess amphiphilic polymers.¹⁸⁻²¹ The heated hydration or the prolonged dialysis may be incompatible with certain functional groups (e.g., maleimide) on polymers for bioconjugation.²² Moreover, these studies used cadmium-based QDs, which have been concerns for biomedical applications and environments.²³⁻²⁴ Loading cadmium-free AIS/ZnS QDs into PLGA-PEG based micelles for biomedical applications is simple and fast and effectively avoids these potential limitations.

EXPERIMENTAL METHODS

Materials and Apparatus

Silver Acetate (99%), Indium (III) Acetate (99.99%), Zinc Stearate (ZnO: 12.5-14%), and Paraformaldehyde (97%) were purchased from Alfa Aesar. Sulfur (>99.99%), Trioctylphosphine (TOP, 90%), 1-Dodecanethiol (98%), 1-Octadecene (ODE, 90%), Oleic Acid (99%), Methanol (99.93%), and 1,10-Phenanthroline (99%) were purchased from Sigma Aldrich. Tetrahydrofuran (THF, >99%), Ethanol (>99%), Chloroform (>99.9%), and Hexane (95%) were purchased from Pharmco-AAPER. Methoxy poly(ethylene glycol)-b-poly(lactide-co-glycolide) (PEG-PLGA) (MW ~ 5000:5000 Da) and maleimide-PEG-PLGA (MW ~ 5000:5000 Da) were purchased from Akina, Inc. Dulbecco's Phosphate Buffered Saline (DPBS), Phosphate Buffered Saline (PBS), Ethylenediaminetetraacetic Acid (EDTA), Acetonitrile (99.96%) and Traut's Reagent were from Fisher Scientific. Heat-inactivated Fetal Bovine Serum (FBS) was from Gibco. U-87 MG and HEK-293 cells were ordered from the American Type Culture Collection (ATCC). RPMI-1640, MEM and DEMEM media were from Corning Cellgro. 7-Aminoactinomycin D dye (7-AAD, excitation at 488 nm and emission at 647 nm) for cell nucleic acid staining was from Invitrogen. Chlorotoxin (CTX) was purchased from Alomone Labs. Bovine Serum Albumin (BSA) was from MP Biomedicals. Zeba spin desalting columns (MWCO 7k) were from Pierces.

The ultraviolet and visible (UV-Vis) spectra of materials were obtained with a UV-Vis spectrometer (UV-2450 from Shimadzu). Photoluminescence spectra of QDs in organic-phase and aqueous-phase were acquired using a spectrophotometer (RF-5301PC from Shimadzu). Photoluminescence intensity of QDs in various buffers was obtained using a microplate reader (PerkinElmer 2030 equipped with a 535 nm emission filter and a 405 nm excitation filter). Transmission electron microscope (TEM) images and Energy-dispersive X-ray (EDX) spectra

were acquired using a JEOL analytical transmission electron microscope (model JEM 2100F operated with a 200 kV acceleration voltage) equipped with an Oxford Energy-Dispersive X-ray (EDX) spectrometer. X-ray Diffraction (XRD) data was collected by a coupled Theta:2-Theta scan on a Rigaku Ultima-III diffractometer equipped with Copper X-ray tube with Ni beta filter, parafocusing optics, computer-controlled slits, and D/Tex Ultra 1D strip detector. The hydrodynamic sizes of micelles were measured using a dynamic light scattering (DLS) instrument (Malvern Zetasizer Nano ZS) equipped with a HeNe laser operating at 632.8 nm and a scattering detector at 173 degrees. Probe sonication was performed with a Misonix ultrasonic processor (QSonica S-4000) equipped with a microtip. Infrared (IR) spectra of materials were collected using a Fourier transform infrared (FT-IR) spectrometer (Perkin-Elmer Frontier) with Spectrum 10 software and the Universal ATR Sampling Accessory. Cells were imaged using a Leica confocal microscope and images were analyzed using ImageJ.

QYs of QDs were calculated according to the following equation, using standard references including Rhodamine 6G (emission peak at 556 nm, QY = 95% in ethanol) and Oxazine 170 (emission peak at 640 nm, QY = 63% in methanol),

$$QY_S = QY_R \times (I_S/I_R) \times (A_R/A_S) \times (n_S/n_R)^2$$

where QY_S and QY_R are the quantum yields of sample and a standard reference, respectively; I_S and I_R are the integrations of fluorescence emissions of sample and a standard reference, respectively; A_S and A_R are the corresponding absorbance of sample and a standard reference, respectively; and n_S and n_R are the refractive indices of the corresponding solvents.

During QY measurements, the absorbance of each sample or each standard reference deviated by less than 0.1. For each sample, the standard reference with the most similar absorption and/or luminescence characteristics was chosen for QY measurements.

AIS/ZnS QD Synthesis

For a typical synthetic reaction, silver acetate (0.1 mmol), Indium (III) acetate (0.2 mmol), DDT (4 mL) and oleic acid (0.2 mmol, 63.5 μ L) were added in a three-necked round bottom flask equipped with a condenser and magnetic stir bar. This mixture was degassed under vacuum for 20 min at 130 °C until the solution became clear. The solution temperature was then increased to 170 °C under a flow of Argon. As the temperature was increased, the color of the reaction solution changed gradually from yellow to orange, indicating the nucleation and growth of AIS QDs. Small amounts of the reaction solution (0.1-0.2 mL) were collected using a syringe at different time intervals and injected into hexane in clean vials to terminate growth of QDs. All solutions collected from the experiment were diluted in a quartz cuvette with hexane for UV–Vis absorbance and photoluminescence measurements. After the reaction was complete, the solution was cooled to room temperature. The crude QDs solution was purified repeatedly with the solvent combinations of hexane/ethanol and chloroform/acetone by centrifugation and dried under vacuum.

For ZnS shell growth, the Zn precursor was prepared by mixing zinc stearate (1.6 mmol) and ODE (4 mL) in a round-bottom flask. The mixture was gradually heated to \sim 100 °C with stirring under vacuum until no vigorous bubbling was observed. The temperature was increased to 160 °C under argon until a clear solution was obtained. The sulfur precursor was prepared by dissolving sulfur (1.6 mmol) in DDT (3.2 mL) and TOP (0.8 mL). The ZnS shell coating of AIS QDs was carried out in situ without purification of the core. 4 mL ODE was added to the crude AIS solution. This core solution was degassed under vacuum at 130 °C for 30 min and then to 210 °C under Argon. Both zinc and sulfur precursors were injected in sequence 5 times to the core growth solution at 210 °C in 0.5 mL portions at 15 min intervals. After reactions were

complete, mixtures were cooled down to room temperature and AIS/ZnS QDs were purified using hexane/ethanol and chloroform/acetone, and dried under vacuum. In our experiments, we can collect around 40 mg AIS QDs and around 100 mg AIS/ZnS QDs per reaction.

Preparation of AIS/ZnS Micelles

The solution of 2.4 mg AIS/ZnS QDs and 9.6 mg PEG-PLGA (50% PEG-PLGA and 50% maleimide-PEG-PLGA) in THF/acetonitrile was layered on the top of cold water in a glass vial. The mixture was ultrasonicated using the Misonix Ultrasonic Liquid Processor with a 3 W output power for 1 min. After sonication, THF/acetonitrile was removed by rotary evaporation at room temperature and the sample filtered through a 0.2 μm syringe filter to remove large aggregates. Empty micelles or single-nanoparticle based micelles were removed by centrifugation at 18,000 rpm for 15 min. The collected micelles were then re-filtered through a 0.2 μm syringe filter, concentrated using a centrifugal filter, dispersed in 400 μL of water, and stored at 4°C until further use.

For CTX conjugation, the thiolation of CTX was completed by dispersing 12.5 nmol of CTX in 100 μL of PBS (pH8, 5 mM EDTA) with 125 nmol of Traut's reagent in 9 μL of PBS (pH 8, 5 mM EDTA) for 1 hour at room temperature. A volume of 87 μL of the prepared micelles in PBS (pH 6.7) was incubated with the thiolated CTX for 2 - 3 hours at room temperature. The resultant CTX-AIS/ZnS micelle product was purified using Zeba spin desalting columns (MWCO 7k) equilibrated with PBS, resuspended in 400 μL of PBS as a stock solution and stored at 4 °C before use. AIS/ZnS micelles without CTX conjugation were used as controls.

Cell Culture, Cellular Uptake/Internalization of AIS/ZnS Micelles, and Cellular Imaging

A U-87 MG human brain glioblastoma cell line (ATCC HTB-14) was maintained in Minimum Essential Media (MEM, Corning Cellgro) supplemented with 10% FBS at 37 °C and 5% CO₂. The human embryonic kidney cell line HEK-293 (ATCC CRL-1537) was maintained in RPMI-1640 medium (Corning Cellgro) supplemented with 10% FBS at 37 °C and 5% CO₂.

For the QD-micelle cellular uptake assay, U-87 and HEK-293 cells were plated on 24-well plastic plates and allowed to propagate for 2-3 days until they reached 50 - 80% confluency. The cells were incubated with CTX-conjugated or non-conjugated AIS/ZnS QD-micelles in cell culture medium with 2% BSA for 2 hours at 37 °C. After incubation, the solution was removed and the cells were washed three times with cold PBS buffer (pH 7.4). Then cells were fixed with 4% paraformaldehyde in PBS at room temperature for 20 min, followed by cell nucleus staining with 7-Aminoactinomycin D (7-AAD) for 45 min. The cells were examined by a laser scanning confocal microscope (LSCM, Leica, TCS SP8, Germany). The statistical significance ($p < 0.05$) was determined by the single-tailed student *t* test.

RESULTS AND DISCUSSION

AIS QDs were produced via a thermal decomposition-based synthesis system with a precursor molar ratio of Ag:In of 1:2. In this system, DDT was used as the sulphur source and the capping ligand as well as the reaction solvent. The thermal decomposition temperature is relatively mild (170 °C).

Figure 1(a) shows photoluminescence spectra of AIS QDs during the time course of growth at 170 °C. It can be seen that the QY of AIS QDs is enhanced during growth reaching 13% at 75 min. The QY enhancement over time is likely caused by a reduction of nanocrystal core defects

during heat treatment. Nevertheless, the photoluminescence spectral shift is not significant or sensitive to growth time. This optical characteristic suggests that AIS growth is very slow. The slow growth of AIS QDs is probably due to the relatively mild reaction temperature. When using a higher reaction temperature (230 °C), typically for CIS QDs, it was found that the products of the AIS synthetic system are hard to solubilize in chloroform and hexane, and thus hard to characterize optically. To further enhance the QY, AIS QDs were passivated with a shell of ZnS to form AIS/ZnS QDs. The AIS/ZnS QDs show a significant QY up to 41% but with a blue shift, as demonstrated in Figure 1(b).

AIS QDs and AIS/ZnS QDs were further characterized using TEM. Figure 2(a) and (b) present TEM and high resolution TEM (HRTEM) images of AIS and AIS/ZnS QDs, respectively. The HRTEM images reveal crystalline patterns and sizes (~4.5 nm for AIS and ~6 nm for AIS/ZnS) of both QDs, indicating that the synthesized particles do be nanocrystals. Energy-dispersive X-ray (EDX) spectra confirm that AIS/ZnS QDs are composed of Ag, In, Zn, and S (Figure 2(c)) and AIS QDs are composed of Ag, In and S (Figure S1). More specifically, Table 1 shows the elemental atomic ratios of AIS and AIS/ZnS QDs. For AIS QDs, the atomic ratio between Ag and In is close to 1:1 with the atomic percentage of In slightly higher. For AIS/ZnS QDs, the atomic percentages of Ag and In drop off but the Ag percentage is reduced to a greater extent, and the atomic percentages of Zn and S are increased. The significant reduction of Ag atomic percentage in AIS/ZnS is probably due to Zn etching to replace Ag during the ZnS shell growth. It is generally agreed that cation exchange between Zn ions (from Zn precursor) with Ag (or Cu) in AIS (or CIS) causes photoluminescence blue shift and QY enhancement.^{8, 25-}

²⁶ As shown in Figure 1(b), we did observed both effects after growing ZnS shell on AIS cores.

EDX analysis demonstrates a good match of the observed photoluminescence blue shift and QD brightness enhancement of AIS/ZnS QDs compared to AIS QDs.

The crystal phase of the AIS and AIS/ZnS QDs was examined by X-ray powder diffraction (XRD), as shown in Figure 3. The XRD pattern of AIS QDs shows three broad peaks at $2\theta = 26.8^\circ$, 44.6° and 52.2° , which can be assigned respectively to the diffractions of the (112), (204) and (312) planes of the tetragonal AgInS_2 . No other phases or impurities were observed. The AIS/ZnS QDs diffraction pattern shows a similar profile to that of the AIS QDs with three right-shifted peaks at 2θ of 27.7° , 46.0° and 54.0° . These peaks can be seen at positions intermediate between the diffractions of (112), (204), and (312) planes of tetragonal AgInS_2 and the diffractions of (111), (220), and (311) planes of cubic ZnS, suggesting that Zn atoms were deposited on or diffused into the surface of the AIS cores.

It should be noted that all characterized materials AIS and AIS/ZnS QDs were synthesized with an original Ag:In precursor molar ratio of 1:2. This ratio is critical to avoid possible side products or black precipitates in reactions. We did synthesize AIS QDs at different Ag:In precursor molar ratios (Ag:In = 1:1, 1:2, and 1:4) without changing other conditions. The collected AIS samples were diluted in hexane and their photoluminescence and UV-Vis absorbance spectra were measured. As shown in Figure S2(a), all samples have similar photoluminescence spectra without obvious shifts. However, as illustrated in Figure S2(b), AIS QDs synthesized with Ag:In = 1:1 have a wider absorbance wavelength range than the other two samples. Moreover, the AIS QD solution (Ag:In = 1:1) is a dark brown color, as illustrated in the inset of Figure S2(b). This suggests that there is something else (i.e., probably Ag_2S) produced during the reaction with Ag:In = 1:1 at 170°C but particles are not large enough to precipitate. The AIS QD solution (Ag:In = 1:1) was further used to grow the ZnS shell on AIS QDs and as

shown in Figure S3(a), the resultant product includes both a green solution and black precipitates. However, after the ZnS shell growth of AIS QDs (Ag:In = 1:2), the resultants are clear (Figure S3(b)). These experimental observations lead to the molar ratio of Ag:In = 1:2 used in the synthesis. We did not investigate the AIS synthesis with Ag:In = 1:4, because this ratio does not significantly shift QD photoluminescence and excess In precursors in the reaction increase synthesis cost.

In the proposed thermal decomposition approach, indium acetate and silver acetate could initially react with DDT to form intermediate compounds of $\text{Ag}(\text{SC}_{12}\text{H}_{25})_x$ and $\text{In}(\text{SC}_{12}\text{H}_{25})_x$ upon heating and are dissolved in DDT.²⁷ As the reaction temperature is raised to 170 °C, the intermediate compounds could act as precursors and further are decomposed into Ag-S and In-S to form Ag-In-S particles. Considering that there are some unexpected materials produced in the reaction with a molar ratio of Ag:In at 1:1, it is possible that $\text{Ag}(\text{SC}_{12}\text{H}_{25})_x$ compounds are decomposed faster than $\text{In}(\text{SC}_{12}\text{H}_{25})_x$ compounds and thus Ag-S are excess to form dark Ag_2S particles. This could explain why 1:2 molar ratio of Ag:In is good for the reaction. Of note, the photostability of the produced AIS and AIS/ZnS QDs were tested and presented in Figure S4.²⁸⁻²⁹ It can be seen that AIS/ZnS QDs remain their photostability but AIS QDs are significantly photobleached. The photobleaching of AIS QDs could be caused by complex UV-induced chemical reactions at the interface between AIS and organic solvents. For example, electrons excited from AIS react with organic solvents to form free radicals which could further etch the AIS surface and quench the AIS photoluminescence. The photostability of AIS/ZnS QDs is believed to benefit from the protection of AIS core by its ZnS shell.

To demonstrate potential biomedical applications of the produced AIS/ZnS QDs, we loaded these QDs into the core of PLGA-PEG based micelles to form QD-micelles. The QD-micelle

preparation is schematically illustrated in Figure 4(a). Briefly, we mixed AIS/ZnS QDs with amphiphilic polymers of PLGA-PEG in organic solvents, and then dispersed them into water with sonication. During the vacuuming or water-replacement of organic solvents, the hydrophobic portion (PLGA) of the polymers and QDs are self-associated into a semi-solid core, and the hydrophilic portion (PEG) of the polymers forms a coronal layer. Photoluminescence spectra of AIS/ZnS QDs before and after water transfer via micelles were measured and are shown in Figure 4(b). It can be seen that the QD-micelles show a slight red-shift in photoluminescence spectra and remain around 30% QY compared to QDs suspended in organic solvents. The red-shift and the QY drop after the phase transfer is believed to be caused by a compact QD cluster in micelle cores.³⁰⁻³¹ In the compact cluster, the emission photons from smaller QDs are absorbed by larger QDs to emit at longer wavelengths (a Förster resonance energy transfer process). Moreover, the cluster reduces the total excitation and emission surface area of QDs, resulting in a QY drop. In spite of quenching, the QD-micelles are still adequate for optical imaging applications. The insets of Figure 4(b) show the hydrodynamic sizes ($126 \text{ nm} \pm 53 \text{ nm}$) of the QD-loaded micelles measured by DLS and the TEM image of QD-micelles, respectively. Figure S5 (a) and (b) show the TEM image and high resolution TEM image of an individual micelle. It can be seen that some dots are presented in a single micelle, and with further zooming into the micelle crystal lattices of dots are observed. Further EDS analysis on micelles (Figure S5 (c)) shows that silver, indium, zinc and sulfur elements are presented in micelles, which are the composites of AIS/ZnS QDs.

For cellular imaging studies, we adopted CTX as a target ligand and used U-87 MG brain tumor cells as model cells. CTX is a 36-amino acid peptide that was originally isolated from scorpion venom, and specifically binds to tumors of neuroectodermal origin.³² Further studies

have demonstrated that CTX is a specific matrix metalloproteinase II (MMP2) inhibitor and can bind with MMP2 present on the surface of glioma cells with high affinity.³³⁻³⁵ The specific binding results in loss of gelatinase activity, disruption in chloride channel currents, reduction in both MMP2 and chloride channel expressions, and internalization of chloride channels. Recent studies have also implicated annexin A2 (ANXA2) as a new recognition target of CTX in multiple tumor cell lines, which may activate similar uptake mechanisms as those of MMP2.³³ U-87 is a human primary glioblastoma cell line expressing MMP2 receptors, and CTX can specifically bind to and be internalized into U-87.³³ In this study, QD-micelles were conjugated with CTX via a maleimide-thiol reaction.³⁶⁻⁴⁰ The CTX conjugation was confirmed by Fourier transform infrared spectroscopy, as shown in Figure 5. The spectrum of the AIS/ZnS QD-micelles exhibits the characteristics of both the alkyl chains in oleic acid and dodecanethiol from AIS/ZnS QDs, corresponding to the CH₂ stretching vibrations peaks at 2922 cm⁻¹ and 2852 cm⁻¹, and the ester carbonyl in PLGA from PLGA-PEG, corresponding to the C=O peaks at 1757 cm⁻¹. After CTX conjugation with the QD-micelles, a new peak at 1650 cm⁻¹ corresponding to the N-H band of primary amines in lysine and arginine residues of CTX,³⁹⁻⁴⁰ appears in the spectrum of CTX-conjugated QD-micelles. This appearance indicates the successful conjugation of CTX with the QD-micelles.

In order to verify that (i) CTX conjugated QD-micelles can be internalized into U-87 cells and (ii) the internalization is due to the CTX-MMP2 interaction, two sets of experiments were performed. In the first, U-87 cells were incubated with CTX conjugated QD-micelles spiked in DEME with 2% BSA for 2 hours. In the second, 400 μM 1,10-phenanthroline was added to DEME, keeping all other conditions same. 1,10-phenanthroline is a broad-spectrum MMP2 inhibitor and can disrupt the MMP2 activity by chelating and removing Zn ions from the

catalytic domain of MMP2.^{33, 41-42} As a result, 1,10-phenanthroline can block the interaction between CTX and MMP2 and thus the sequential cellular internalization process.

After incubation, the U-87 cells from two sets of experiments were washed, fixed, stained and imaged. Representative confocal images shown in Figure 6(a-d) demonstrate the cellular uptake/internalization of CTX-conjugated QD-micelles by U-87 cells. The representative confocal images in Figure 6(e-h) illustrate the quenching effect of 1,10-phenanthroline on uptake/internalization. Figure 6(i) shows quantitative data (the fluorescence intensity from the internalized QD-micelles per unit cytoplasm area counting > 200 cells) comparing cellular uptake/internalization and the quenching effect under the different concentrations or dilutions of CTX-conjugated QD-micelles (100 - 800 times dilution). These results demonstrate that the internalization of CTX-conjugated QD-micelles into U-87 cells is caused by an interaction between CTX and MMP2.

To further confirm that CTX-conjugated QD-micelles is specific to U-87, we used human embryonic kidney 293 cells (HEK-293), a nonmalignant cell line that does not express MMP2 and ANXA2 on cell surfaces, as controls to examine their response to QD-micelles conjugated with/without CTX and compared to those of U-87. Figure 7(a-b) and 7(c-d) show the representative cellular uptake images (overlaid confocal images) for U-87 and HEK-293, respectively, under the same QD-micelle concentration or dilution. Figure 7(e) shows fluorescence intensity (from the internalized QD-micelles) per unit cytoplasm area under a series of dilutions of QD-micelles stock solutions. It can be seen that U-87 cells do internalize more CTX-conjugated QD-micelles than HEK-293, and non-conjugated QD-micelles produce no significant cellular uptake by both cell lines. Through this comparison, it can be concluded that CTX-conjugated QD-micelles are specific to U-87. Interestingly, we also observed that HEK-

293 did internalize some CTX-conjugated QD-micelles at a high concentration. Some pioneer work has reported that CTX can increase the rate of pinocytic internalization.^{33, 43} We believe that the cellular uptake of CTX-conjugated micelles may involve pinocytosis mechanisms in high concentration ranges.

Using PLGA-PEG to wrap AIS/ZnS QDs is an effective approach for phase transfer and bio-applications. We believe that the AIS/ZnS QD-micelles as image contrasts or probes can be used to detect endogenous targets expressed on brain tumor cells, or more broadly to cell- or tissue-based diagnosis and therapy.

CONCLUSION

In summary, a thermal decomposition-based synthesis was developed to produce AIS and AIS/ZnS QDs. Without involving highly toxic precursors, the synthesis method is both simple and safe. The resultant AIS and AIS/ZnS QDs present 13% and 41% QYs, respectively. To render AIS/ZnS QDs for biomedical applications, amphiphilic polymers PLGA-PEG were used to encapsulate AIS/ZnS QDs to form QD-micelles in a manner that is simple and fast. Further cellular studies show that CTX-conjugated QD-micelles can be specifically internalized into U-87 brain tumor cells. We believe that the scalable synthesis of AIS/ZnS QDs and the facile surface/interface chemistry for phase transfer and bioconjugation of these QDs open avenues for the QD-micelles to serve as a powerful platform for broader biomedical applications, especially for cell- or tissue-based diagnosis and therapy. Our future work will focus on (i) further developing AIS and AIS/ZnS QDs with high QYs and a wide photoluminescence range by adjusting nonstoichiometric compositions or doping additional elements into these QDs within a

thermal decomposition system, and (ii) exploring the potential applications of the QD-micelles in image-guided drug delivery.

ACKNOWLEDGEMENT

This research was supported by the National Institute of Health via grant #1P20GM103650.

REFERENCES

1. H. Zhong, Z. Bai, B. Zou, *J. Phys. Chem. Lett.* 2012, 3, 3167.
2. T. Torimoto, T. Kameyama, S. Kuwabata, *J. Phys. Chem. Lett.*, 2014, 5, 336.
3. R. Xie, M. Rutherford, X. Peng, *J. Am. Chem. Soc.*, 2009, 131, 5691.
4. R. Buonsanti, D.J. Milliron, *Chem. Mater.*, 2013, 25, 1305.
5. T. Ogawa, T. Kuzuya, Y. Hamanaka, K. Sumiyama, *Journal of Materials Chemistry*, 2010, 20, 2226.
6. J. Chang, G. Wang, C. Cheng, W. Lin, J. Hsu, *J. Mater. Chem.*, 2012, 12, 10609.
7. M. Dai, S. Ogawa, T. Kameyama, K. Okazaki, A. Kudo, S. Kuwabata, Y. Tsuboi, T. Torimoto, *J. Mater. Chem.*, 2012, 22, 12851.
8. B. Mao, C. Chuang, F. Lu, L. Sang, J. Zhu, C. Burda, *J. Phys. Chem. C*, 2013, 117, 648.
9. H. Shinchu, M. Wakao, N. Nagata, M. Sakamoto, E. Mochizuki, T. Uematsu, S. Kuwabata, Y. Suda, *Bioconjugate Chem.*, 2014, 25, 286.
10. G. Gabka, P. Bujak, K. Giedyk, A. Ostrowski, K. Malinowska, J. Herbich, B. Colec, I. Wielgus, A. Pron, *Inorg. Chem.*, 2014, 53, 5002.
11. B. Mao, C. Chuang, C. McCleese, J. Zhu, C. Burda, *J. Phys. Chem. C*, 2014, 118, 13883.

12. Y. J. Park, J. H. Oh, N. S. Han, H. C. Yoon, S. M. Park, Y. R. Do, J. K. Song, *J. Phys. Chem. C*, 2014, 118, 25677.
13. B. Mei, K. Susumu, I. Medintz, J. Delehanty, T. Mountziaris, H. Mattoussi, *J. Mater. Chem.*, 2008, 18, 4949.
14. J. Delehanty, J. Blanco-Canosa, C. Bradburne, K. Susumu, M. Stewart, D. Prasuhn, P. Dawson, I. Medintz, *Chem. Commun.*, 2013, 49, 7878.
15. K. Susumu, H. Uyeda, I. Medintz, T. Pons, J. Delehanty, H. Mattoussi, *J. Am. Chem. Soc.*, 2007, 129, 13987.
16. H. Uyeda, I. Medintz, J. Jaiswal, S. Simon, H. Mattoussi, *J. Am. Chem. Soc.*, 2005, 127, 3870.
17. M.F. Foda, L. Huang, F. Shao, H.Y. Han, *ACS Appl. Mater. Interfaces*, 2014, 6, 2011.
18. B. Dubertret, P. Skourides, D. J. Norris, V. Noireaus, A. H. Brivanlou, A. Libchaber, *Science*, 2002, 298, 1759.
19. E.F. Erogbogbo, K.T. Yong, R. Hu, W.C. Law, H. Ding, C.W. Chang, P.N. Prasad, M.T. Swihart, *ACS Nano*, 2010, 4, 5131.
20. J.H. Park, G. von Maltzahn, E. Ruoslahti, S.N. Bhatia, M.J. Sailor, *Angew. Chem.*, 2008, 120, 7394.
21. B.-S. Kim, T.A. Taton, *Langmuir*, 2007, 23, 2198.
22. S. Tong, S. Hou, B. Ren, Z. Zheng, G. Bao, *ACS Nano*, 2011, 11, 3720.
23. B. A. Rzigalinski, J. S. Strobl *Toxicol. Appl. Pharmacol.*, 2009, 238, 280.
24. R. Hardman, *Health Perspect.*, 2006, 114, 165.
25. J. Park, S. W. Kim, *J. Mater. Chem.*, 2011, 21, 3745.

26. L. D. Trizio, M. Prato, A. Genovese, A. Casu, M. Povia, R. Simonutti, M. J. P. Alcocer, C. D'Andrea, F. Tassone, L. Manna, *Chem. Mater.*, 2012, 24, 2400.
27. H. Zhong, Y. Zhou, M. Ye, Y. He, J. Ye, C. He, C. Yang, Y. Li, *Chem. Mater.*, 2008, 20, 6434.
28. J. Wei, J. Qiu, L. Ren, K. Zhang, S. Wang, B. Weeks, *Sci. Adv. Mater.*, 2014, 6, 1052.
29. P. Jiang, C.-N. Zhu, Z.-L. Zhang, Z.-Q. Tian, D.-W. Pang, *Biomaterials*, 2012, 33, 5130.
30. M. Booth, R. Peel, R. Partanen, N. Hondow, V. Vasilca, L. J. C. Jeuken, K. Critchley, *RSC Adv.*, 2013, 3, 20559.
31. R. Shrake, V. G. Demillo, M. Ahmadiantehrani, X. Zhu, N. G. Publicover, K. W. Hunter Jr., *J. Colloid Interface Sci.*, 2015, 437, 140.
32. S. A. Lyons, J. O'Neal, H. Sontheimer, *Glia*, 2002, 39, 162.
33. J. L. Kovar, E. Curtis, S. F. Othman, M. A. Simpson, D. M. Olive, *Anal. Biochem.*, 2013, 440, 212.
34. J. Deshane, C. C. Garner, H. Sontheimer, *J. Biol. Chem.*, 2003, 278, 4135.
35. K. Kesavan, J. Ratliff, E. W. Johnson, W. Dahlberg, J. M. Asara, P. Misra, J. V. Frangioni, D. B. Jacoby, *J. Biol. Chem.*, 2010, 285, 4366.
36. R. L. Orndorff, S. J. Rosenthal, *Nano Lett.*, 2009, 9, 2589.
37. R. Huang, W. Ke, L. Han, J. Li, S. Liu, C. Jiang, *Biomaterials*, 2011,32, 2399.
38. C. Fang, O. Veiseh, F. Kievit, N. Bhattarai, F. Wang, Z. Stephen, C. Li, D. Lee, R. G. Ellebogen, M. Zhang, *Nanomedicine*, 2010,5, 1357.
39. C. Sun, C. Fang, Z. Stephen, O. Veiseh, S. Hansen, D. Lee, R. G. Ellenbogen, J. Olson, M. Zhang, *Nanomedicine*, 2008,3, 495.

40. C. Sun, O. Veiseh, J. Gunn, C. Fang, S. Hansen, D. Lee, R. Sze, R. G. Ellenbogen, J. Olson, M. Zhang, *Small*, 2008,4, 372.
41. J. Hu, X. Zhang, W. B. Nothnick, T. E. Spencer, *Biol. Reprod.*, 2004, 71, 1598.
42. G. Soslau, C. Mason, S. Lynch, J. Benjamin, D. Ashak, J. M. Prakash, A. Moore, P. Bagsiyao, T. Albert, L. M. Mathew, M. Jost, *Thromb Haemost.*, 2014,111, 140.
43. E. M. Burns, G. D. Dobben, T. W. Krukeberg, P. K. Gaetano, *Adv. Neurol.*, 1981,30, 159.

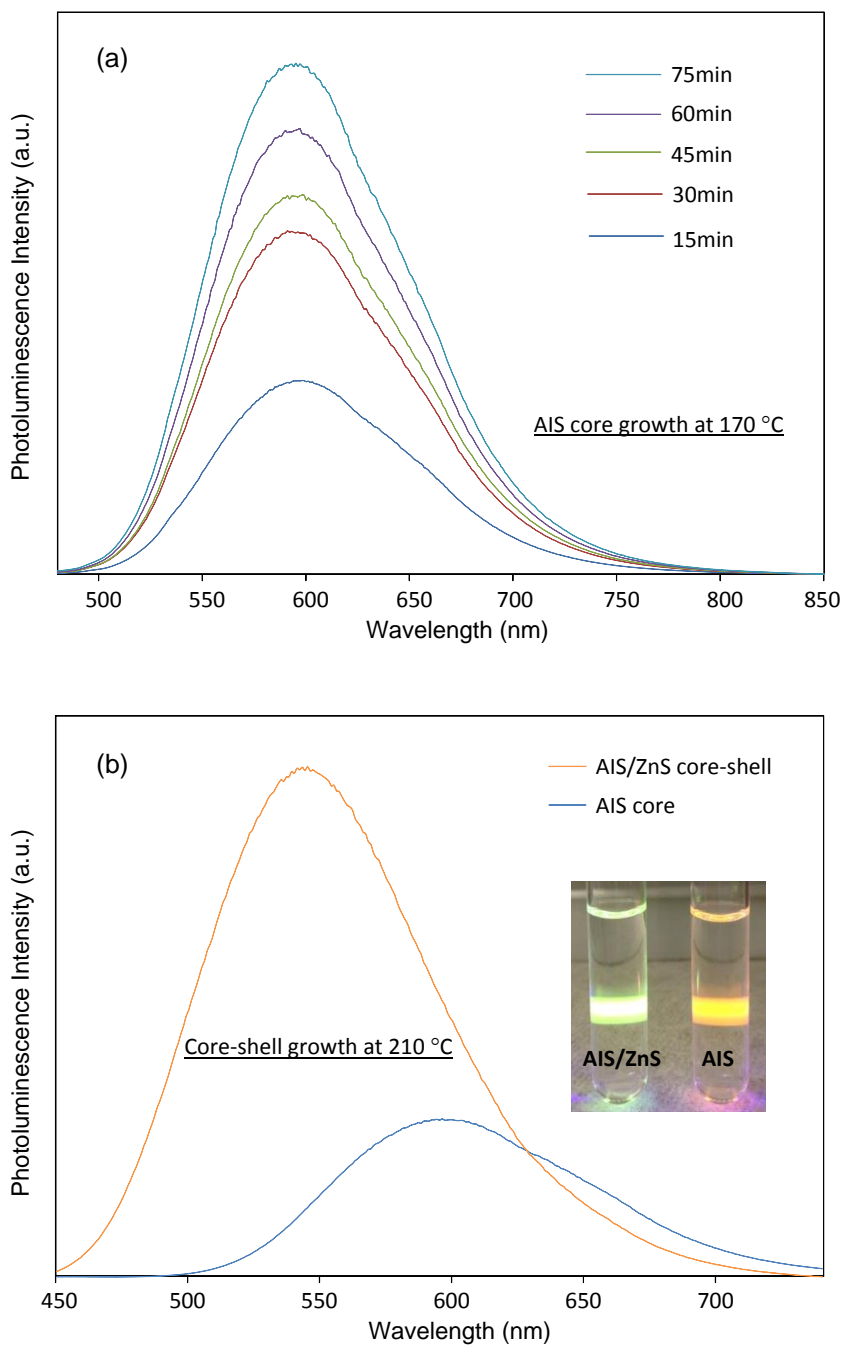
FIGURES, TABLES AND CAPTIONS

Figure 1. (a) Evolution of the photoluminescence spectra of AIS QDs during the time course of growth at 170 °C; (b) Photoluminescence spectra of AIS QDs and AIS/ZnS QDs where the inset shows a digital photograph of AIS QDs and AIS/ZnS QDs in organic solvents exposed under a UV laser beam. Note that in (a) and (b), all photoluminescence spectra of QDs are scaled by their quantum yields.

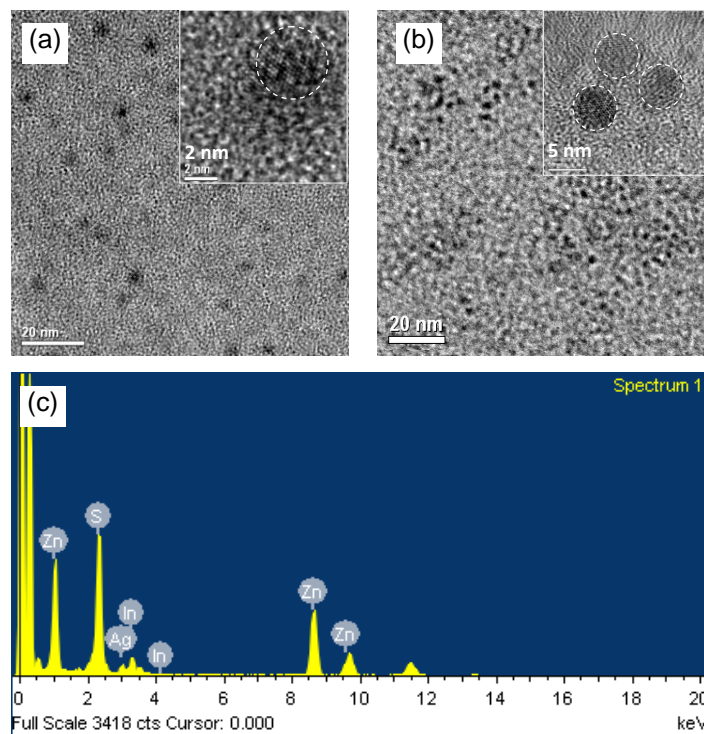


Figure 2. (a) TEM and high resolution TEM images of AIS QDs; (b) TEM and high resolution TEM images of AIS/ZnS QDs; (c) EDX spectrum of AIS/ZnS illustrating Ag, In, Zn and S elements.

Table 1. Element atomic ratio (EDX analysis), quantum yields (QYs) and photoluminescence (PL) peak wavelengths of AIS and AIS/ZnS QDs

Synthesis Conditions	Measured Atomic Ratio by EDX				QY (%)	PL Peak (nm)
	Zn	Ag	In	S		
AIS	-	21.3	27.6	51.1	13	594
AIS/ZnS	29.7	3.4	6.4	60.5	41	545

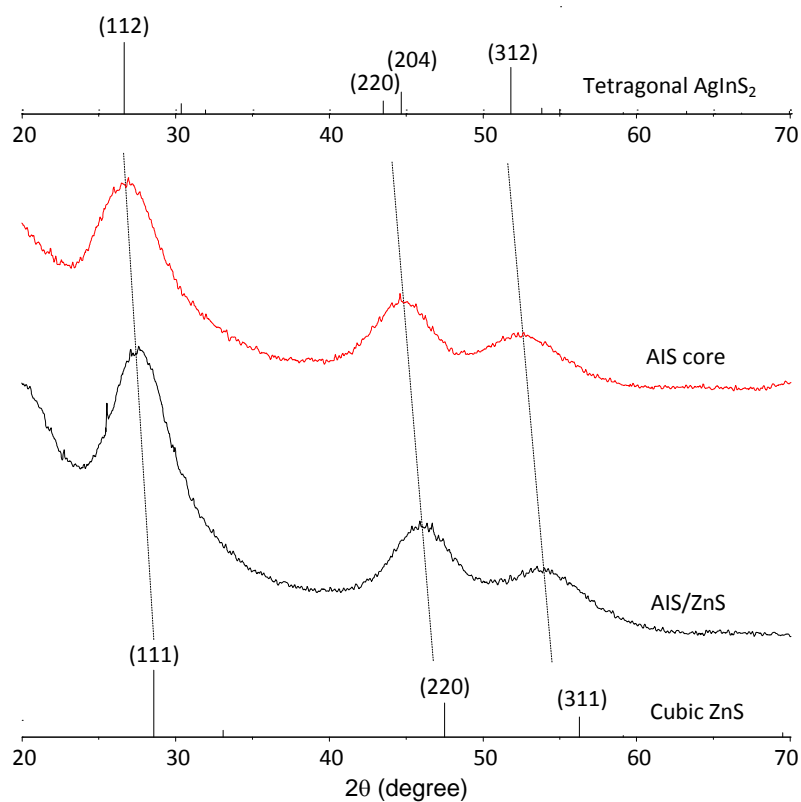


Figure 3. XRD patterns for AIS and AIS/ZnS QDs. Diffraction peaks of tetragonal AgInS_2 and cubic ZnS, as obtained from ICDD/ICSD 04-007-4439 and ICDD/ICSD 01-077-3378, are shown as references.

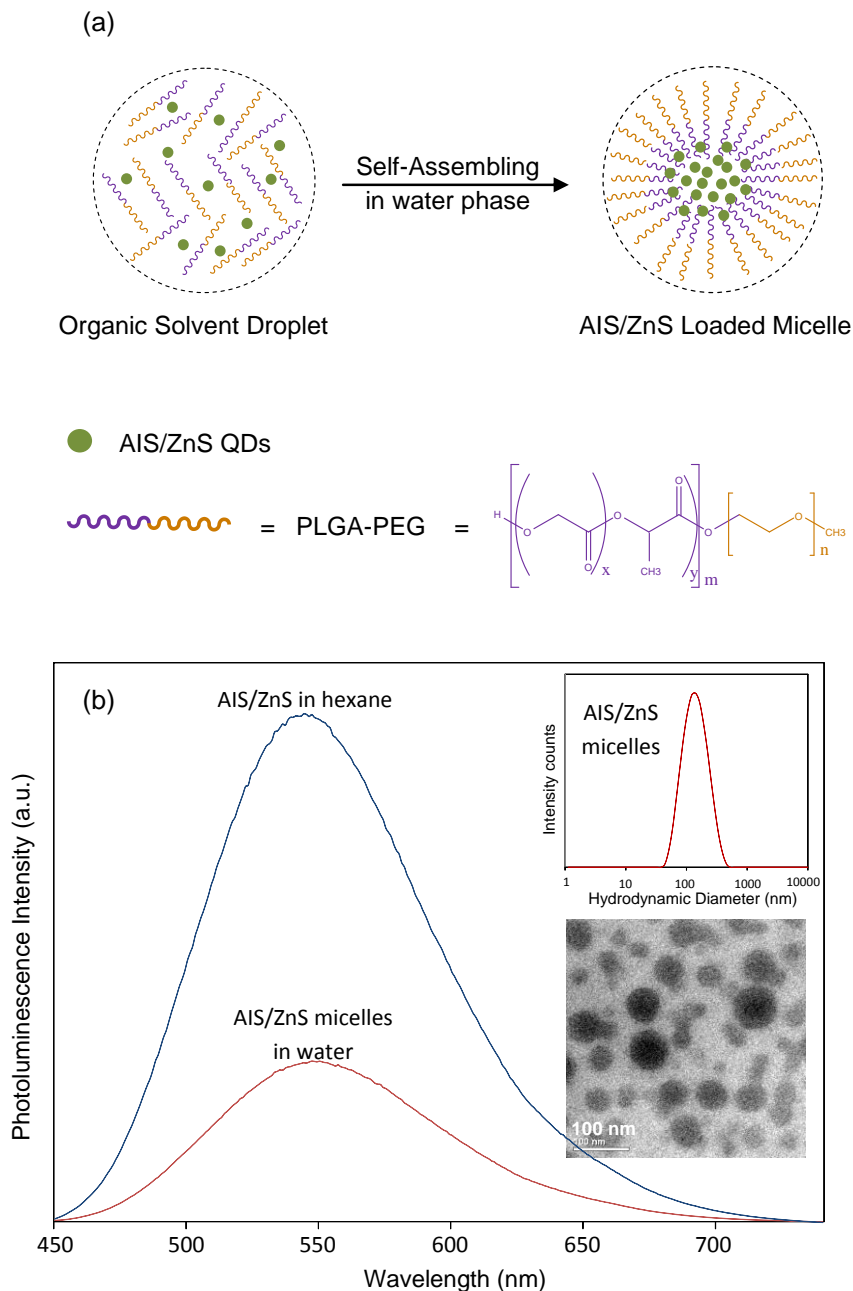


Figure 4. (a) Fabrication scheme of the AIS/ZnS loaded micelles using PLGA-PEG (5k:5k) and AIS/ZnS QDs; (b) Photoluminescence spectra of AIS/ZnS QDs in hexane and AIS/ZnS micelles in water. The photoluminescence spectra of QDs and micelles are scaled according to their quantum yields. Insets are the hydrodynamic size distribution of the resulting AIS/ZnS QD-micelles measured by DSL (top) and the corresponding TEM image of QD-micelles (bottom), respectively.

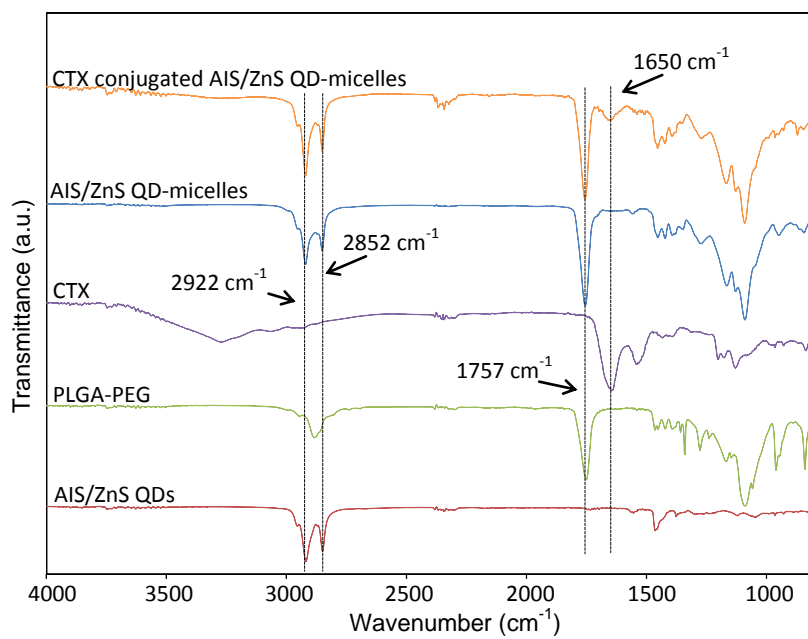


Figure 5. FTIR spectra of AIS/ZnS QDs, PLGA-PEG, CTX, QD-micelles, and CTX conjugated QD-micelles.

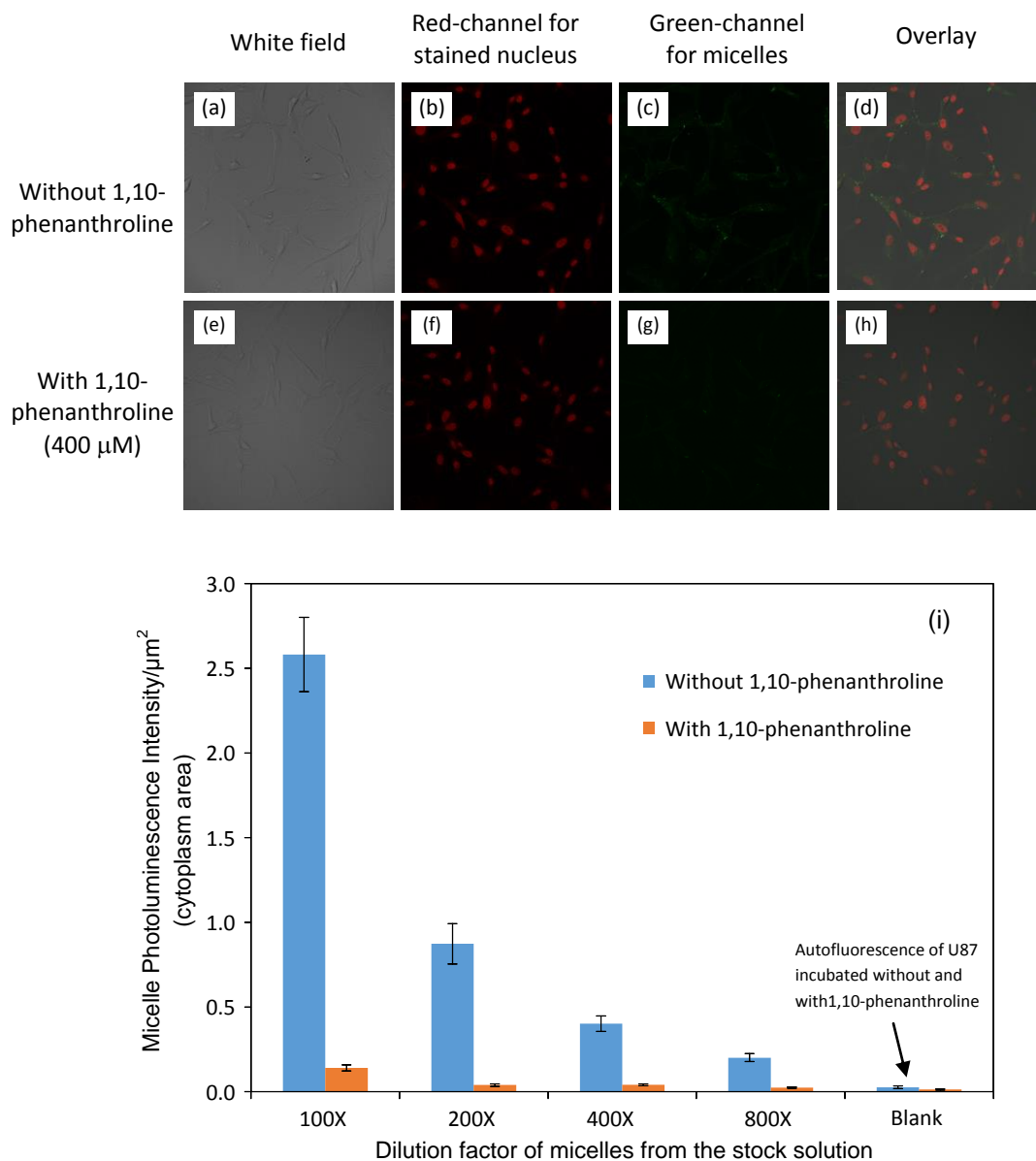


Figure 6. (a-d) Confocal images demonstrating the cellular uptake/internalization of CTX-conjugated QD-micelles (100 times diluted from stock) by U-87 cells; (e-h) Confocal images presenting the quenching effect of 1,10-phenanthroline on the uptake/internalization; (i) Quantitative data indicating the cellular uptake/internalization and the quenching effect under the different concentrations or dilutions of CTX-conjugated QD-micelles (100 - 800 times dilutions). All *p* values for each comparison are less than 0.01.

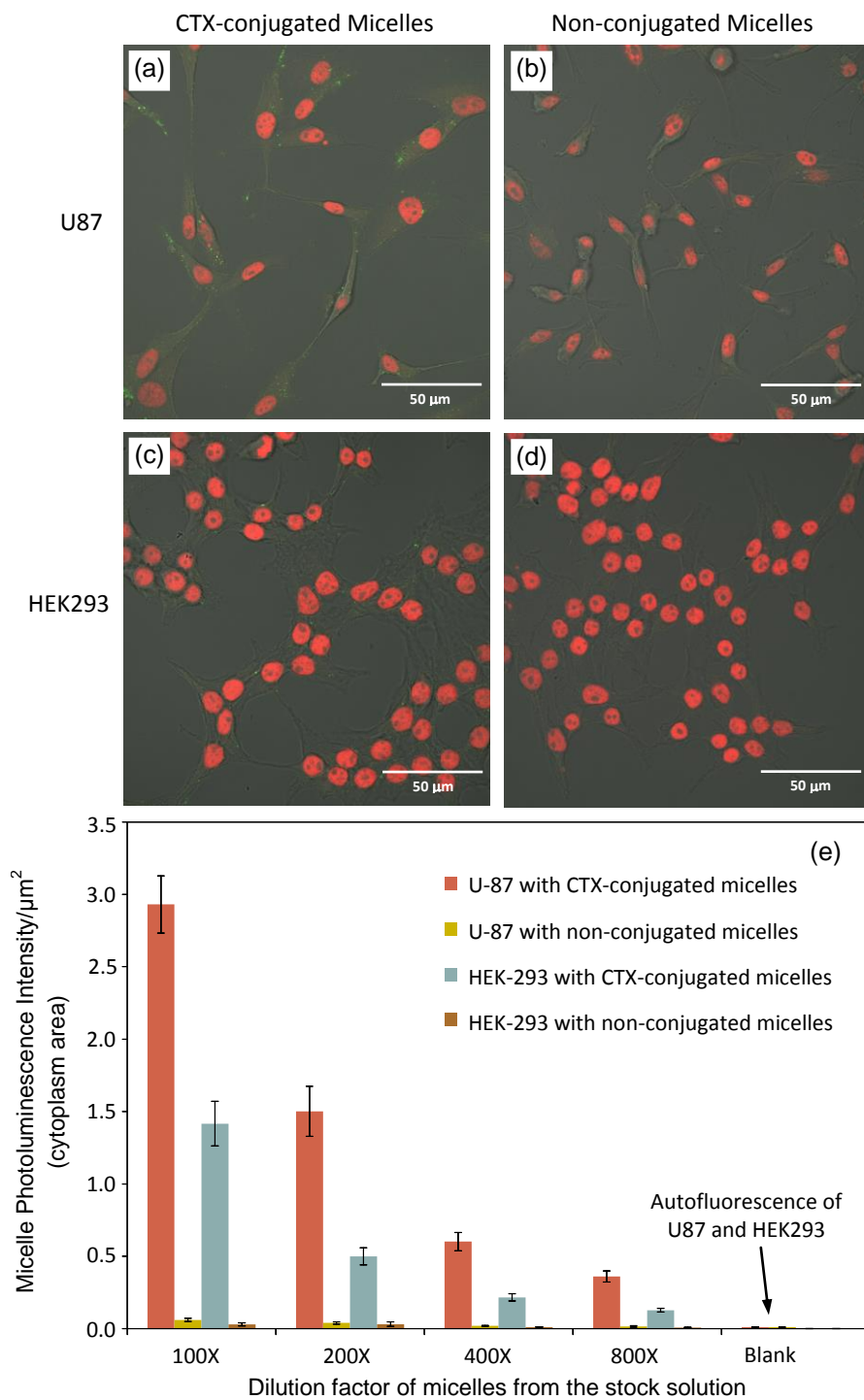


Figure 7. (a-d) Overlaid confocal images of U-87 cells and HEK-293 cells after incubating with CTX-conjugated and non-conjugated micelles (200 times diluted from each stock), respectively; (e) Fluorescent intensity per unit area of cytoplasm for U-87 and HEK-293 cells incubated with CTX-conjugated and non-conjugated AIS/ZnS micelles. All p values for each comparison are less than 0.01.